

Contents lists available at ScienceDirect

China University of Geosciences (Beijing)

Geoscience Frontiers

journal homepage: www.elsevier.com/locate/gsf

Research paper

SHRIMP zircon dating and LA-ICPMS Hf analysis of early Precambrian rocks from drill holes into the basement beneath the Central Hebei Basin, North China Craton



Yusheng Wan ^{a,b,c,*}, Xianzheng Zhao ^d, Zejiu Wang ^e, Dunyi Liu ^{a,b}, Alfred Kröner ^b, Chunyan Dong ^{a,b}, Hangqian Xie ^{a,b}, Yuansheng Geng ^a, Yuhai Zhang ^{a,b}, Runlong Fan ^{a,b}, Huiyi Sun ^{a,b}

^a Institute of Geology, Chinese Academy of Geological Sciences, Beijing 100037, China^b Beijing SHRIMP Center, Institute of Geology, Chinese Academy of Geological Sciences, Beijing 100037, China^c State Key Laboratory for Continental Tectonics and Dynamics, Institute of Geology, Chinese Academy of Geological Sciences, Beijing 100037, China^d North China Oilfield Company of PetroChina, Rengiu 062552, China^e Chinese Academy of Geological Sciences, Beijing 100037, China

ARTICLE INFO

Article history:

Received 9 January 2014

Received in revised form

17 February 2014

Accepted 21 February 2014

Available online 15 March 2014

Keywords:

Early Precambrian

North China Craton

Drill hole

Zircon dating

Hf isotopic analysis

ABSTRACT

The Central Hebei Basin (CHB) is one of the largest sedimentary basins in the North China Craton, extending in a northeast–southwest direction with an area of >350 km². We carried out SHRIMP zircon dating, Hf-in-zircon isotopic analysis and a whole-rock geochemical study on igneous and metasedimentary rocks recovered from drill holes that penetrated into the basement of the CHB. Two samples of gneissic granodiorite (XG1-1) and gneissic quartz diorite (J48-1) have magmatic ages of 2500 and 2496 Ma, respectively. Their zircons also record metamorphic ages of 2.41–2.51 and ~2.5 Ga, respectively. Compared with the gneissic granodiorite, the gneissic quartz diorite has higher ΣREE contents and lower Eu/Eu* and (La/Yb)_n values. Two metasedimentary samples (MG1, H5) mainly contain ~2.5 Ga detrital zircons as well as late Paleoproterozoic metamorphic grains. The zircons of different origins have ε_{Hf} (2.5 Ga) values and Hf crustal model ages ranging from 0 to 5 and 2.7 to 2.9 Ga, respectively. Therefore, ~2.5 Ga magmatic and Paleoproterozoic metasedimentary rocks and late Neoproterozoic to early Paleoproterozoic and late Paleoproterozoic tectono-thermal events have been identified in the basement beneath the CHB. Based on regional comparisons, we conclude that the early Precambrian basement beneath the CHB is part of the North China Craton.

© 2014, China University of Geosciences (Beijing) and Peking University. Production and hosting by Elsevier B.V. All rights reserved.

1. Introduction

Geological, geochemical and geochronological studies revealed many common features in the exposed early Precambrian rocks of

the North China Craton (NCC) (Wan et al., 2011a; Zhai and Santosh, 2011; Zhao and Zhai, 2013 and references therein), which are summarized as follows: (1) the NCC underwent a long and complex tectono-magmatic history back to 3.8 Ga, with 2.8–3.8 Ga rocks having been identified in several areas; (2) juvenile additions of crust from mantle sources were generated in the late Mesoarchean to early Neoarchean and constitute an important crust formation event; (3) the NCC is different from several other cratons in having experienced extensive late Neoarchean tectono-thermal events that resulted in recycling of more ancient crustal material, besides juvenile crustal additions; (4) all or parts of the NCC experienced an extensional tectonic event during the latest Neoarchean as a mark of cratonic stabilization; (5) Paleoproterozoic geological processes in the NCC were much more complex than thought before, with 2.4–2.49 Ga metamorphism and 2.0–2.35 Ga magmatism having

* Corresponding author. Institute of Geology, Chinese Academy of Geological Sciences, Beijing 100037, China.

E-mail address: wanyusheng@bjshrimp.cn (Y. Wan).

Peer-review under responsibility of China University of Geosciences (Beijing)



Production and hosting by Elsevier

been identified in many areas; (6) late Paleoproterozoic (1.8–1.95 Ga) tectono-thermal events occurred widely in the NCC and led to a unified craton towards the end of the Paleoproterozoic. However, the NCC is extensively covered by Mesoproterozoic and younger sedimentary sequences. Zircon dating of rocks recovered from drill holes into the basement was carried out in only a few basins. One such study revealed late Paleoproterozoic magmatism and metamorphism in basement rocks beneath the Songliao basin in the northeastern NCC (Pei et al., 2007), whereas another study indicated that the Ordos basement in the western NCC was involved in a widespread late Paleoproterozoic tectono-thermal event (Hu et al., 2012; Wan et al., 2013).

The Central Hebei Basin (CHB) is one of the largest basins in the NCC, and we carried out SHRIMP zircon dating, Hf-in-zircon isotopic analysis and a whole-rock geochemical study of magmatic and metasedimentary rocks recovered from drill holes that penetrated its basement.

2. Geological background

The CHB extends in a northeast–southwest direction with an area of >350 km² (Fig. 1). Its basement is entirely covered by Mesoproterozoic and younger sedimentary rocks. Based on drill core data and geophysical investigations (NCOCP, 2012), the basement is composed of magmatic (mainly granitoids) and supracrustal rocks (mainly amphibolite, biotite plagioclase gneiss and schist) with greenschist- to upper amphibolite-facies metamorphism and local anatexis. The bottom of the basin shows up-and-down elevations with the greatest depth being >5000 m. In some areas the early Precambrian basement constitutes buried hills that are controlled by northeast–southwest faults and extend roughly in the same direction as the basin.

Early Precambrian rocks occur extensively around the CHB. In the northwest and west of the basin there are the early Precambrian Fuping and Zanhuang complexes that contain 1.8–1.9,

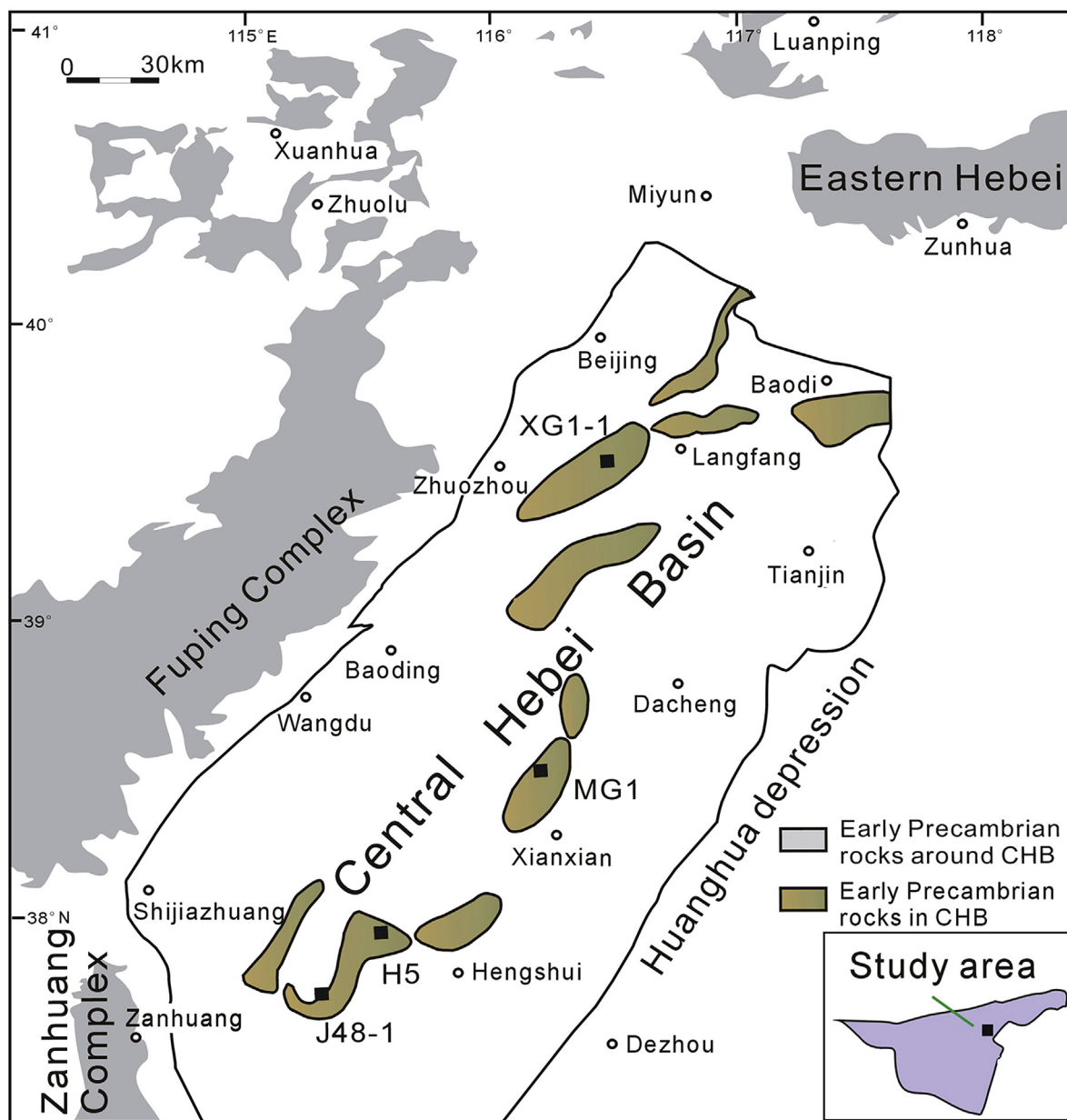


Figure 1. Geological map of the Central Hebei Basin and surrounding areas (modified after NCOCP, 2012), showing sample locations in this study. The identification of early Precambrian rocks within the Central Hebei Basin is based on drill core data and geophysical investigations.

2.0–2.2, 2.5–2.55 and ~2.7 Ga granitoids and 1.83–1.92 Ga metamorphic rocks (Zhao et al., 2000, 2002; Guan et al., 2002; Cheng et al., 2004; Yang et al., 2004, 2011a, 2011b, 2013; Trap et al., 2008, 2009; Xiao et al., 2011; Han et al., 2012). In eastern Hebei, northeast of the basin, Archean supracrustal and magmatic rocks occur widely (Liu et al., 1992, 2013; Geng et al., 2006; Yang et al., 2008; Wilde et al., 2008; Sun et al., 2010; Nutman et al., 2011; Zhang et al., 2011, 2012a, 2012b). In the southeast of the basin is the Huanghua depression beneath which basement rocks are also suspected. Four samples for this study were obtained from drill holes that went up to one or more than 10 m into the basement rocks. The locations are shown in Fig. 1, and general information about the samples is provided in Table 1. The petrographic features are summarized below.

2.1. Gneissic granodiorite (XG1-1)

This sample was taken from a drill hole in the northeastern portion of the basin. It shows a gneissic structure (Fig. 2a) and consists of plagioclase, quartz and biotite. Fine-grained plagioclase occurs as aggregates and is altered to epidote and sericite with some phenocrysts showing polysynthetic twinning. Some fine-grained dirty grains may be K-feldspar, but this is difficult to determine under the microscope. Quartz grains are coarser-grained than feldspar, show undulose extinction and are oriented as aggregates parallel to feldspar aggregates, defining a strong foliation. There are fine aggregates of chlorite as a result of alteration of biotite.

2.2. Anatetic biotite K-feldspar paragneiss (MG1)

This sample comes from a drill hole in the central portion of the basin. The rock is inhomogeneous and shows an anatetic texture with K-feldspar-rich leucosome batches (Fig. 2b). It is composed of feldspar, quartz and biotite. Feldspar is dirty (probably sericitized) and is considered to be mainly K-feldspar because the rock contains high K₂O and low Na₂O (Table 1). Some quartz grains are oriented as aggregates. Biotite occurs as aggregates parallel to quartz aggregates and is partly altered to chlorite. It is difficult to determine the protolith of the rock because of strong deformation, metamorphism and anatexis. We prefer a sedimentary origin because of high K₂O and low Na₂O (although this is partly due to the analyzed sample containing leucosome) and that it is interlayered with garnet two-feldspar paragneiss (NCOCP, 2012).

2.3. Muscovite-bearing K-feldspar quartzite (H5)

This sample is from a drill core in the southwestern portion of the basin and shows a layered structure (Fig. 2c). The rock is mainly composed of quartz and K-feldspar with some muscovite. Quartz is

fine-grained and shows a triple junction texture. K-feldspar occurs as small grains or porphyroclasts. Fine-grained muscovite flakes are scattered between quartz grains but show orientation, and some muscovite seems to have formed by alteration of K-feldspar. These features suggest that the rock underwent recrystallization after strong deformation.

2.4. Gneissic quartz diorite (J48-1)

This sample was taken from a drill hole about 30 km southwest of sample H5. The rock is gray in color and shows a weak gneissic structure (Fig. 2d). It is mainly composed of plagioclase, quartz and biotite. Plagioclase is strongly altered to sericite and epidote. Some feldspar grains show weaker alteration and are considered to be K-feldspar. Many biotite flakes are altered to chlorite and a dark mineral. Quartz does not occur as aggregates, and this suggests that the rock did not undergo strong deformation.

3. Analytical techniques

Major oxides were analyzed by XRF and trace elements by ICPMS in the Institute of Geological Analysis, Chinese Academy of Geological Science (CAGS), Beijing. Uncertainties for XRF and ICPMS are estimated at 3–5% and 3–8%, respectively.

Zircon dating was carried out on the SHRIMP II ion microprobe at the Beijing SHRIMP Center, Institute of Geology, CAGS. The analytical procedures were similar to those described by Williams (1998). Five scans through the mass stations were made for each age determination. The intensity of the primary ion beam was 3–4 nA. Primary beam size was ~30 μm, and each site was rastered for 120–200 s prior to analysis. Standards M257 (U = 840 ppm, Nasdala et al., 2008) and TEMORA 1 (²⁰⁶Pb/²³⁸U age = 417 Ma; Black et al., 2003) were used for calibration of U abundance and ²⁰⁶Pb/²³⁸U ratio respectively. The TEMORA 1 to unknown ratio was 1:3–4. Data processing and assessment was carried out using the SQUID and ISOPLOT programs (Ludwig, 2001, 2003). The measured ²⁰⁴Pb was used for common lead correction. ²⁰⁷Pb/²⁰⁶Pb ratios were used to assess the age of all samples. The uncertainties for individual analyses are quoted at the 1σ level, whereas uncertainties on weighted mean ages are quoted at the 95% confidence level.

In-situ zircon Hf isotopic analyses were conducted on a Finnigan Neptune MC-ICPMS with a NewWave UP213 laser ablation microprobe at the Institute of Mineral Resources, CAGS. The detailed analytical procedures were described by Hou et al. (2007). Analyses were carried out using a laser beam diameter of 55 μm. The standard GJ-1 zircon was analyzed to check for instrument reliability and stability. Calculation of $\epsilon_{\text{Hf}}(t)$ values was based on a decay constant for ¹⁷⁶Lu of $1.867 \times 10^{-11} \text{ a}^{-1}$ (Söderlund et al., 2004) and

Table 1

Nature and location of early Precambrian rock samples from drill cores beneath the Central Hebei Basin, North China Craton.

Sample No.	Rock name	Location	Depth (m)	Weight (kg)	Main minerals	Protolith	Formation (deposition or intrusion) age (Ga)
XG1-1	Gneissic granodiorite	North of basin, ~30 km west of Lanfang	4795–4798	0.9	Plagioclase, quartz, K-feldspar	Magmatic rock	~2.5
MG1	Anatetic biotite K-feldspar gneiss	Central basin, ~30 km northwest of Xianxian	2481–2487	1.5	Quartz, K-feldspar, biotite	Detrital sedimentary rock	1.8–2.5
H5	Muscovite-bearing K-feldspar quartzite	South of basin, ~40 km northwest of Hengshui	Uncertain	0.7	Quartz, K-feldspar, muscovite	Detrital sedimentary rock	1.8–2.5
J48-1	Gneissic quartz diorite	South of basin, ~55 km west of Hengshui	1855–1857	0.7	Plagioclase, K-feldspar, quartz, biotite	Magmatic rock	~2.5



Figure 2. Photographs of early Precambrian rocks obtained from drill cores into the basement beneath the Central Hebei Basin, North China Craton. (a) Gneissic granodiorite (XG1-1); (b) anatetic biotite K-feldspar paragneiss (MG1); (c) muscovite-bearing K-feldspar quartzite (H5); (d) gneissic quartz diorite (J48-1). The coin is ~1.5 cm in diameter.

the present-day chondritic ratios of $^{176}\text{Hf}/^{177}\text{Hf} = 0.282772$ and $^{176}\text{Lu}/^{177}\text{Hf} = 0.0332$ (Blichert-Toft and Albarède, 1997). Two-stage Hf model ages (crustal model ages $t_{\text{DM2(CC)}}$) were calculated by assuming a mean $^{176}\text{Lu}/^{177}\text{Hf}$ value of 0.01 (Kröner et al., 2014), rather than 0.015 (Griffin et al., 2000) for the average continental crust.

4. Zircon dating

4.1. Gneissic granodiorite (XG1-1)

The zircons are stubby, elliptical or round in shape and show complex textures in cathodoluminescence (CL) images (Fig. 3a–c). Magmatic zircons show oscillatory zoning and recrystallization to different degrees. The recrystallized domains can be subdivided into two types, inner dark and outer light domains. Some light domains show weak zoning, but others are homogeneous. It cannot be excluded that some light domains are overgrowth rims. It is evident that the rounded terminations are not the original shapes of the zircons but resulted from “metamorphic corrosion”, a typical feature in medium to high-grade metamorphic rocks due to dissolution of the pyramidal terminations (Kröner et al., 2013). This indicates that the relationships between outer shape and inner texture cannot be used as indicators of zircon origins. Twenty-one analyses were taken on 18 zircons (Table 2). Three analyses on magmatic domains yielded U contents and Th/U ratios of 155–267 ppm and 0.58–0.86, two of these have a weighted mean $^{207}\text{Pb}/^{206}\text{Pb}$ age of 2500 ± 15 Ma (MSWD = 0.004) (Fig. 4a), which is taken as the formation age of the granodiorite. Eleven analyses on recrystallized dark domains have U contents and Th/U ratios of 265–1015 ppm and 0.29–1.64 and show a variation in $^{207}\text{Pb}/^{206}\text{Pb}$

age from 2386 to 2511 Ma, except for spot 12.1RC(d) which has a $^{207}\text{Pb}/^{206}\text{Pb}$ age of 2189 Ma because of strong lead loss. Four analyses plot on or near concordia with the youngest ages yielding a weighted mean $^{207}\text{Pb}/^{206}\text{Pb}$ age of 2412 ± 17 Ma (MSWD = 1.9), which is considered to record a tectono-thermal event at the early Paleoproterozoic. Seven analyses on recrystallized light domains have much lower U contents (13–21 ppm) and higher Th/U ratios (1.75–4.44) than the dark ones and show a similar age variation to the dark domains but with large errors due to low U contents. The variations in U contents and Th/U ratios resulted from redistribution of U and Th in the recrystallized parts of magmatic zircons. However, some recrystallized grains almost entirely became light domains, suggesting that U and Th were removed from the zircons with U easier to be removed than Th, probably under fluid conditions.

4.2. Anatetic biotite K-feldspar paragneiss (MG1)

The detrital zircons are stubby with rounded terminations and show complex textures in CL images (Fig. 3d–f). The cores show oscillatory zoning, but most show recrystallization. It is difficult to determine when the inner light domains underwent recrystallization (before or after deposition), but we treat them as cores. Sixteen analyses on the cores yielded U contents and Th/U ratios of 152–1574 ppm and 0.22–1.26, excepting 6.1D and 20.1D which have Th/U ratios of 3.14 and 6.41 (Table 2) probably due to analysis spots on Th-high mineral inclusions. They show strong lead loss but define a discordia line with an upper intercept age of ~2.5 Ga (Fig. 4b). Analysis 2.2D is on an inherited core and has a $^{207}\text{Pb}/^{206}\text{Pb}$ age of 2634 Ma (Fig. 3e, grain 2). This suggests that the magmatic rocks in the source region at least partly contained older

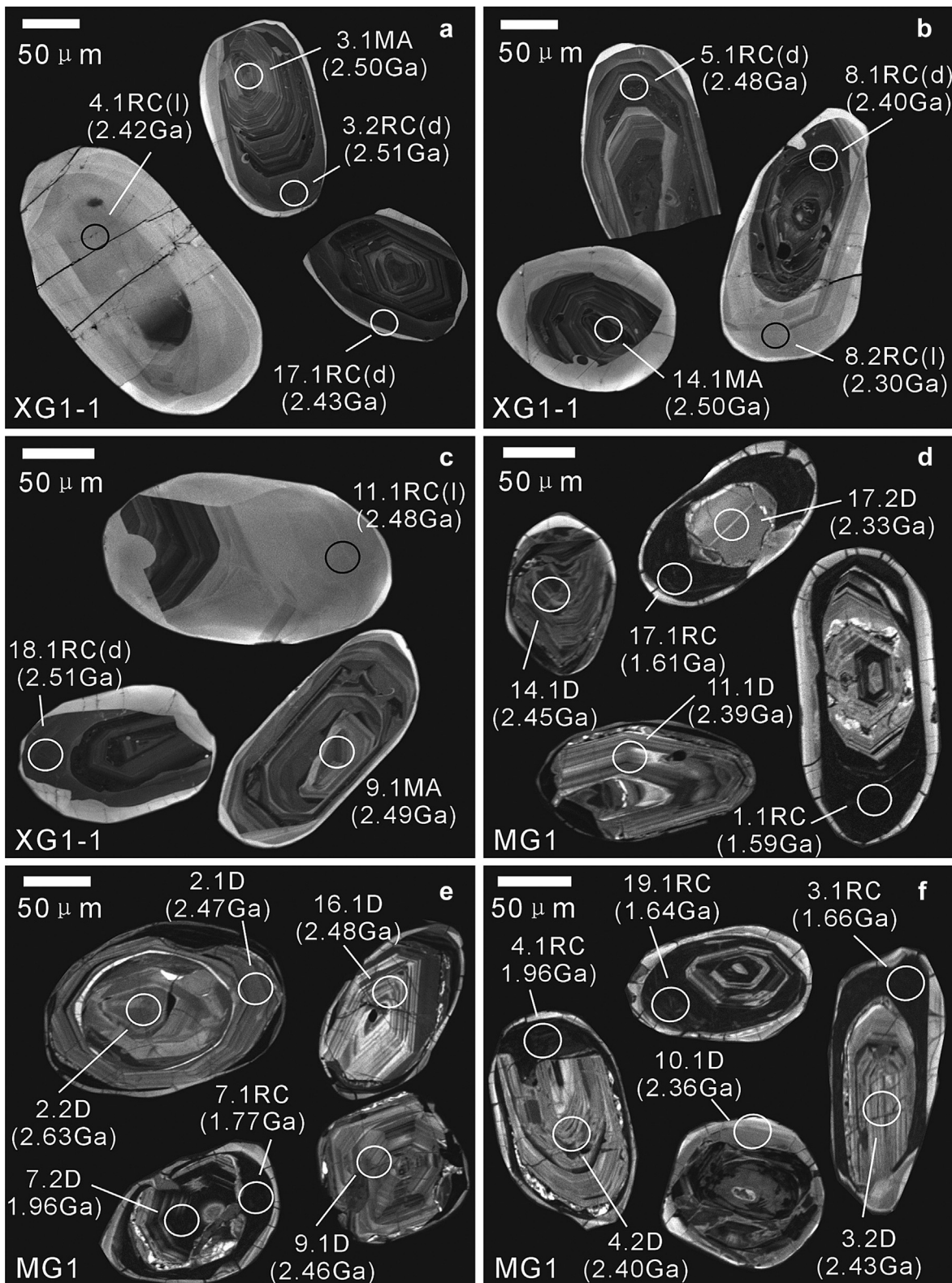
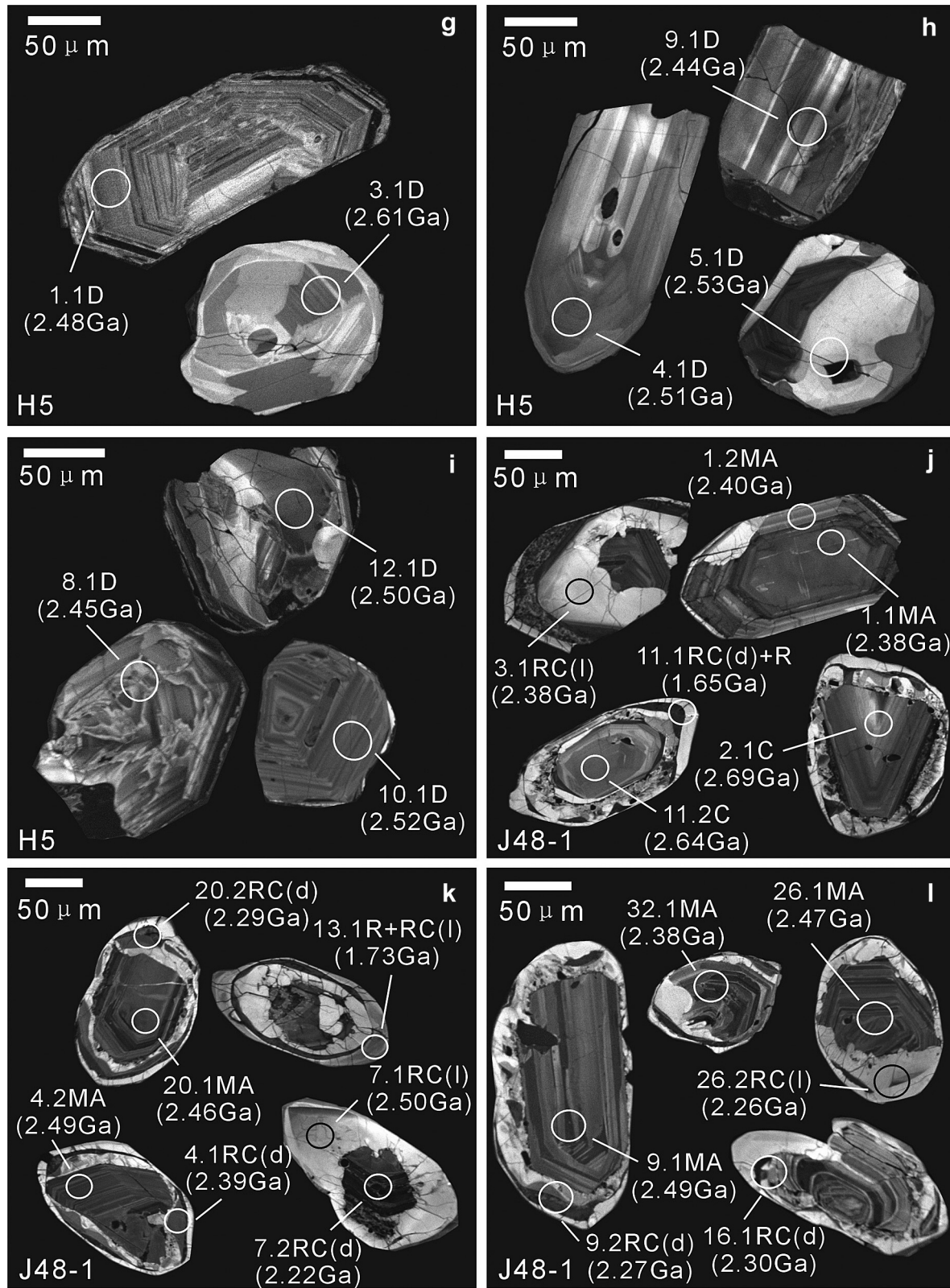


Figure 3. Cathodoluminescence images of zircons from early Precambrian rocks obtained from drill cores into the basement beneath the Central Hebei Basin, North China Craton. (a)–(c) Gneissic granodiorite (XG1-1); (d)–(f) anatetic biotite K-feldspar paragneiss (MG1); (g)–(i) muscovite-bearing K-feldspar quartzite (H5); (j)–(l) gneissic quartz diorite (J48-1). MA, D, C, RC(d) and RC(I) represent magmatic, detrital and core zircons and recrystallized dark and light domains, respectively.

continental material. The outer dark domains look like overgrowth rims, but some show blurred zoning (Fig. 3d, grain 17; Fig. 3f, grain 19), indicating that they formed by recrystallization, probably under fluid conditions. Seven analyses on the dark domains have U

contents and Th/U ratios of 841–2268 ppm and 0.09–0.44 (Table 2). They show stronger lead loss than the cores, and no precise ages could be obtained. We speculate that recrystallization was related to a tectono-thermal event at the end of the

**Figure 3.** (continued).

Paleoproterozoic because no tectono-thermal event <1.8 Ga has so far been reported in the central NCC. The outermost light “rims” are also considered to have formed as a result of recrystallization during which U and Th were redistributed between the light and dark domains.

4.3. Muscovite-bearing K-feldspar quartzite (H5)

Besides their shapes, the zircons show large variations in internal texture, such as oscillatory zoning (Fig. 3g, grain 1), banded zoning (Fig. 3h, grain 9), sector zoning (Fig. 3g, grain 3) or strong

Table 2
SHRIMP U-Pb data for zircons from early Precambrian rocks from drill cores beneath the Central Hebei Basin, North China Craton.

Spot	$^{206}\text{Pb}_{\text{c}}$ (%)	U (ppm)	Th (ppm)	Th/U	$^{206}\text{Pb}^*$ (ppm)	$^{207}\text{Pb}^*/^{206}\text{Pb}^*$ ±%	$^{207}\text{Pb}^*/^{235}\text{U}$ ±%	$^{206}\text{Pb}^*/^{238}\text{U}$ ±%	Errcorr	$^{206}\text{Pb}/^{238}\text{U}$ age	$^{207}\text{Pb}/^{206}\text{Pb}$ age	Discordant (%)
Gneissic granodiorite (XG1-1)												
1.1RC(d)	0.23	684	218	0.33	263	0.1632	0.62	10.05	1.8	0.447	2380	±34
1.2RC(l)	—	20	67	3.43	9	0.1559	3.6	10.51	4.5	0.488	2563	±56
2.1RC(l)	1.68	13	25	1.96	5	0.1469	6.5	8.60	7.1	0.422	2271	±57
3.1MA	0.01	155	87	0.58	65	0.1642	0.58	11.09	1.9	0.490	2569	±38
3.2RC(d)	0.05	347	100	0.30	135	0.1649	0.39	10.25	1.8	0.451	2399	±35
4.1RC(l)	—	21	89	4.44	9	0.1567	1.6	10.21	3.7	0.472	2493	±68
5.RC(d)	0.06	1015	635	0.65	400	0.1620	0.23	10.25	1.7	0.459	2434	±35
6.1RC(d)	—	690	1092	1.64	248	0.1536	0.27	8.85	1.7	0.418	2250	±33
7.1RC(l)	0.42	15	28	1.89	7	0.1712	2.2	12.16	4.5	0.515	2678	±85
8.1RC(d)	0.13	409	246	0.62	160	0.1552	0.35	9.77	1.8	0.457	2424	±35
8.2RC(l)	—	21	78	3.76	9	0.1457	3.8	9.18	5.4	0.456	2424	±77
9.1MA	0.16	180	127	0.73	74	0.1631	0.73	10.74	2.0	0.477	2516	±39
10.1RC(d)	0.13	292	177	0.63	112	0.1578	0.72	9.67	1.9	0.444	2370	±35
11.1RC(l)	—	19	65	3.52	9	0.1625	3.3	11.73	4.3	0.523	2711	±62
12.1RC(d)	—	934	560	0.62	195	0.1368	0.50	4.56	1.8	0.242	1395	±21
13.1RC(l)	1.07	16	27	1.75	7	0.1498	6.2	9.54	6.9	0.461	2443	±65
14.1MA	0.24	267	221	0.86	110	0.1643	0.69	10.83	1.9	0.478	2519	±37
15.1RC(d)	—	336	215	0.66	128	0.1560	0.39	9.52	1.8	0.443	2363	±34
16.1RC(d)	0.01	265	92	0.36	120	0.1637	0.46	11.84	1.8	0.525	2720	±39
17.1RC(d)	—	334	93	0.29	131	0.1575	0.92	9.92	2.0	0.457	2425	±36
18.1RC(d)	0.07	324	125	0.40	136	0.1654	0.51	11.11	1.8	0.487	2560	±38
Anatectic biotite K-feldspar gneiss (MG1)												
1.1RC	0.40	2268	201	0.09	388	0.0983	0.84	2.69	1.7	0.198	1166	±16
2.1D	0.37	276	166	0.62	84	0.1611	0.85	7.82	1.8	0.352	1944	±26
2.2D	0.34	257	136	0.55	82	0.1779	0.78	9.04	1.8	0.369	2022	±28
3.1RC	0.56	1389	199	0.15	226	0.1020	0.59	2.65	1.6	0.189	1113	±16
3.2D	0.34	390	218	0.58	94	0.1577	0.71	6.04	1.8	0.278	1582	±23
4.1RC	0.47	841	236	0.29	162	0.1205	0.52	3.70	1.6	0.223	1297	±18
4.2D	0.22	547	412	0.78	148	0.1550	0.42	6.70	1.6	0.314	1759	±24
5.1D	0.43	217	142	0.68	67	0.1628	0.71	8.06	1.7	0.359	1979	±27
6.1D	0.41	194	590	3.14	65	0.1651	1.3	8.86	2.0	0.389	2119	±29
7.1RC	0.56	1314	301	0.24	240	0.1083	0.72	3.16	1.7	0.212	1237	±17
7.2D	0.68	1053	954	0.94	205	0.1200	0.75	3.72	1.7	0.225	1306	±18
8.1RC	0.69	1857	654	0.36	283	0.1016	0.77	2.47	1.7	0.176	1045	±15
9.1D	0.32	530	401	0.78	80	0.1605	0.75	3.88	1.8	0.175	1040	±15
10.1D	0.11	1574	341	0.22	537	0.1510	0.19	8.26	1.6	0.397	2155	±28
11.1D	0.35	440	383	0.90	81	0.1535	0.57	4.54	1.6	0.215	1253	±17
12.1D	0.34	262	220	0.87	73	0.1630	1.1	7.26	1.9	0.323	1805	±24
13.1D + RC	0.42	548	224	0.42	119	0.13945	0.55	4.82	1.6	0.251	1441	±20
14.1D	0.16	864	308	0.37	175	0.15910	0.51	5.15	1.6	0.235	1360	±19
15.1D + RC	0.43	383	329	0.89	109	0.1527	0.66	6.93	1.7	0.329	1834	±25
16.1D	0.61	152	186	1.26	42	0.1626	1.3	7.06	2.1	0.315	1766	±26
17.1RC	1.01	1596	244	0.16	267	0.09924	0.90	2.63	1.8	0.193	1135	±16
17.2D	0.26	509	306	0.62	116	0.1484	0.76	5.43	1.7	0.266	1518	±21
18.1D	0.80	736	342	0.48	121	0.1485	0.81	3.87	1.8	0.189	1117	±16
19.1RC	0.96	1558	663	0.44	275	0.1006	1.1	2.82	1.9	0.203	1193	±16
20.1D	0.62	637	3955	6.41	87	0.1410	1.1	3.08	1.9	0.158	948	±14
Muscovite-bearing K-feldspar quartzite (H5)												
1.1D	0.75	296	103	0.36	63	0.1626	0.91	5.48	2.3	0.244	1409	±27
2.1D	1.47	518	320	0.64	47	0.1476	1.3	2.14	2.5	0.105	643	±13
3.1D	1.19	30	47	1.63	13	0.1751	2.8	11.70	3.8	0.485	2547	±56
4.1D	0.64	60	46	0.79	24	0.1652	1.5	10.64	2.8	0.467	2471	±49
5.1D	1.10	52	44	0.87	17	0.1668	1.5	8.52	2.9	0.370	2031	±42
6.1D	1.04	47	36	0.78	20	0.1641	1.8	11.07	3.1	0.489	2568	±52
7.1D	0.75	304	439	1.49	58	0.1604	0.93	4.86	2.3	0.220	1280	±25
8.1D	2.48	508	377	0.77	79	0.1597	1.4	3.89	2.6	0.177	1050	±21
9.1D	1.44	274	200	0.75	35	0.1584	1.8	3.22	2.9	0.147	2452	±24
10.1D	0.30	181	139	0.80	46	0.1658	1.5	6.68	2.7	0.292	1652	±33
11.1D	3.18	80	150	1.94	20	0.1541	2.9	5.96	3.8	0.280	1594	±34
12.1D	0.84	407	320	0.81	54	0.1603	10	3.38	2.4	0.153	917	±18
13.1D	1.18	58	65	1.16	16	0.1681	2.5	7.17	3.5	0.309	1736	±37
14.1D	0.36	176	138	0.81	42	0.1626	0.97	6.17	2.4	0.275	1567	±31
15.1D	0.90	149	234	1.62	47	0.1606	1.1	8.10	2.5	0.366	2010	±38
16.1D	2.99	767	590	0.80	105	0.1406	1.7	3.00	2.7	0.155	928	±19
17.1D	1.23	171	206	1.25	51	0.1554	1.6	7.36	2.8	0.344	1903	±37
18.1D	0.77	98	143	1.51	31	0.1612	1.5	8.15	2.9	0.367	2015	±42

(continued on next page)

Table 2 (continued)

Spot	$^{206}\text{Pb}_c$ (%)	U (ppm)	Th (ppm)	Th/U	$^{206}\text{Pb}^*$ (ppm)	$^{207}\text{Pb}^*/^{206}\text{Pb}^*$	$\pm\%$	$^{207}\text{Pb}^*/^{235}\text{U}$	$\pm\%$	$^{206}\text{Pb}^*/^{238}\text{U}$	$\pm\%$	Errcorr	$^{206}\text{Pb}/^{238}\text{U}$ age	$^{207}\text{Pb}/^{206}\text{Pb}$ age	Discordant (%)		
Gneissic quartz diorite (J48-1)																	
1.1MA	0.11	495	179	0.36	110	0.1519	0.48	5.42	2.9	0.259	2.9	0.99	1484	± 38	2368	± 8	37
1.2MA	0.44	442	162	0.37	117	0.1546	1.1	6.51	2.1	0.305	1.8	0.86	1715	± 27	2400	± 18	29
2.1C	0.21	76	39	0.53	32	0.184	0.85	12.51	2.2	0.493	2.0	0.92	2583	± 42	2690	± 14	4
3.1RC(l)	3.62	26	1	0.03	5	0.1516	6.2	4.27	6.5	0.203	2.7	0.41	1190	± 29	2376	± 100	50
4.1RC(d)	—	314	85	0.28	49	0.1540	0.82	3.83	1.9	0.180	1.8	0.91	1067	± 17	2392	± 14	55
4.2MA	0.19	285	132	0.48	101	0.1630	0.57	9.27	1.8	0.412	1.8	0.95	2226	± 33	2487	± 10	11
5.1RC(d)	1.51	687	170	0.26	64	0.1208	2.3	1.79	2.9	0.107	1.7	0.61	655	± 11	1973	± 41	67
6.1RC(l) + R	0.98	418	19	0.05	35	0.1177	2.6	1.55	3.1	0.095	1.8	0.58	585	± 10	1927	± 45	70
7.1RC(l)	0.35	46	1	0.02	16	0.1637	1.3	8.91	2.5	0.394	2.1	0.84	2143	± 38	2495	± 22	14
7.2RC(d)	0.48	646	336	0.54	80	0.1392	1.2	2.75	2.1	0.143	1.7	0.83	861	± 14	2220	± 20	61
8.1C	0.07	197	87	0.46	83	0.1718	0.48	11.55	1.9	0.488	1.8	0.97	2560	± 38	2576	± 8	1
9.1MA	0.75	243	139	0.59	81	0.1632	0.48	8.69	1.8	0.386	1.8	0.97	2104	± 31	2489	± 8	15
9.2RC(d)	2.54	457	40	0.09	39	0.1430	1.5	1.92	2.5	0.097	2.0	0.79	597	± 11	2267	± 26	74
10.1RC(l)	1.32	213	15	0.07	30	0.1353	1.8	3.00	2.5	0.160	1.8	0.71	958	± 16	2172	± 31	56
11.1RC(d) + R	2.50	464	16	0.04	15	0.1006	5.5	0.51	5.7	0.037	1.9	0.33	232	± 4	1646	± 100	86
11.2C	0.04	118	72	0.63	53	0.1787	0.69	12.97	2.0	0.526	1.9	0.94	2725	± 41	2642	± 11	–3
12.1RC(l)	0.84	94	3	0.03	21	0.1540	2.4	5.34	3.1	0.251	1.9	0.64	1444	± 25	2396	± 40	40
12.2MA	—	347	314	0.93	86	0.1658	0.68	6.58	1.9	0.288	1.8	0.93	1631	± 25	2516	± 11	35
13.1R + RC(l)	—	1106	328	0.31	31	0.1054	1.7	0.47	2.4	0.032	1.7	0.72	206	± 4	1726	± 31	88
14.1MA	0.08	224	106	0.49	85	0.1646	0.46	9.99	1.8	0.440	1.8	0.97	2352	± 35	2503	± 8	6
15.1MA	0.55	153	131	0.89	55	0.1625	0.65	9.38	2.0	0.419	1.9	0.95	2255	± 36	2482	± 11	9
16.1RC(d)	1.37	213	66	0.32	35	0.1454	1.2	3.82	2.1	0.190	1.8	0.84	1122	± 18	2296	± 20	51
17.1MA	0.98	368	169	0.47	76	0.1553	0.58	5.11	1.9	0.238	1.8	0.95	1379	± 22	2405	± 10	43
18.1RC(d)	0.93	296	164	0.57	87	0.1626	0.49	7.62	1.8	0.340	1.7	0.96	1886	± 29	2484	± 8	24
19.1RC(l)	0.66	40	1	0.02	15	0.1669	1.8	9.83	3.4	0.427	2.9	0.86	2290	± 56	2529	± 29	9
20.1MA	—	263	167	0.66	75	0.1604	0.61	7.27	2.0	0.329	1.9	0.95	1831	± 31	2460	± 10	26
20.2RC(d)	0.74	386	41	0.11	36	0.1448	1.4	2.14	2.4	0.107	1.9	0.81	654	± 12	2288	± 24	71
21.1RC(d)	1.30	337	46	0.14	46	0.1447	0.90	3.14	2.0	0.157	1.8	0.89	940	± 16	2285	± 15	59
22.1RC(d)	0.87	465	9	0.02	48	0.1314	1.4	2.17	2.3	0.119	1.8	0.79	727	± 12	2120	± 24	66
23.1RC(d)	0.12	311	154	0.51	38	0.1361	1.7	2.64	2.8	0.141	2.2	0.79	848	± 17	2182	± 30	61
24.1RC(d)	—	279	20	0.07	40	0.1482	1.2	3.36	2.2	0.164	1.8	0.83	980	± 16	2327	± 21	58
25.1RC(d)	0.37	740	149	0.21	29	0.1108	2.3	0.68	2.9	0.045	1.8	0.61	281	± 5	1819	± 41	85
26.1MA	—	198	142	0.74	76	0.1617	0.63	9.88	1.9	0.443	1.8	0.94	2363	± 36	2474	± 11	4
26.2RC(l)	—	43	10	0.24	13	0.1423	4.0	6.78	4.6	0.345	2.5	0.53	1909	± 41	2261	± 68	16
27.1RC(l)	0.64	104	33	0.33	23	0.1547	1.5	5.47	3.2	0.256	2.8	0.88	1469	± 37	2400	± 25	39
28.1RC(l)	1.75	193	52	0.28	18	0.1268	3.5	1.91	3.9	0.109	2.0	0.50	665	± 12	2060	± 59	68
29.1MA	1.05	271	121	0.46	69	0.1595	0.98	6.49	2.0	0.295	1.8	0.88	1667	± 26	2451	± 16	32
30.1RC(d)	—	392	338	0.89	94	0.1568	0.70	6.00	1.9	0.278	1.8	0.94	1579	± 26	2422	± 12	35
31.1MA	0.06	520	331	0.66	88	0.1402	0.84	3.78	1.9	0.195	1.7	0.90	1150	± 18	2232	± 14	48
32.1MA	—	397	307	0.80	77	0.1529	0.81	4.75	1.9	0.225	1.8	0.91	1309	± 21	2381	± 14	45

Note: (1) Common lead corrected using measured ^{204}Pb ; (2) $^{206}\text{Pb}^*$ is radiogenic lead; (3) Discordance(%) is defined as $[(1 - (^{206}\text{Pb}/^{238}\text{U})\text{age})/(^{207}\text{Pb}/^{206}\text{Pb})\text{age}] \times 100$; (4) age in Ma; (5) MA, D, C, RC(d) and RC(l) represent magmatic, detrital and core zircons and recrystallized dark and light domains, respectively.

recrystallization (**Fig. 3h**, grain 5; **Fig. 3i**, grains 8 and 12). Eighteen analyses yielded U contents and Th/U ratios of 30–767 ppm and 0.36–1.94 (**Table 2**) and exhibit lead loss to different degrees but plot roughly on a discordia line with 3 analyses on concordia (**Fig. 4c**). It is evident that the source region(s) are mainly composed of ~2.5 Ga rocks. Some zircons have metamorphic rims, but these are too narrow for SHRIMP analysis (**Fig. 3h**, grain 5; **Fig. 3i**, grain 12). We consider that metamorphism occurred at the end of the Paleoproterozoic for the same reason as mentioned for sample MG1.

4.4. Gneissic quartz diorite (J48-1)

The magmatic zircons are stubby in shape and show oscillatory zoning but with most undergoing recrystallization (**Fig. 3j–l**). Two recrystallized domains can be subdivided. One is homogeneous and light gray in CL images (**Fig. 3j**, grain 3; **Fig. 3k**, grain 7), another is inhomogeneous with light and dark intergrowths that commonly occur in the outermost domains of zircons (**Fig. 3j**, grains 2 and 11; **Fig. 3l**, grain 9). Forty-nine analyses were carried out on 32 zircons (**Table 2**). Thirteen analyses on magmatic domains have U contents of 153–520 ppm and Th/U ratios of 0.36–0.93. They show strong lead loss but define a discordant line with 7 analyses closest to concordia yielding an upper intercept age of 2496 ± 14 Ma

(MSWD = 1.7) (**Fig. 4d**) that is interpreted as the intrusive age of the quartz diorite. Thirteen analyses on inhomogeneous, dark domains have U contents of 279–740 ppm and Th/U ratios of 0.02–0.89. Eight analyses on the homogeneous, light domains have U contents of 26–213 ppm and Th/U ratios of 0.02–0.33, being lower than the magmatic domains. This is different from the zircons of sample XG1-1 in which the recrystallized, light domains have much higher Th/U ratios than magmatic domains, probably indicating that their recrystallization occurred under different conditions (mainly fluid composition, redox condition, pH value and temperature). The analyses on recrystallized domains plot on the same discordia line as the analyses on magmatic domains. Therefore, we consider that the rock underwent metamorphism soon after its formation. There are also trapped 2576–2690 Ma zircon cores (**Fig. 3j**, grains 2 and 11; **Fig. 4d**).

5. Geochemistry and Hf-in-zircon isotopes

5.1. Whole-rock compositions

The chemical analyses of the dated rock samples are listed in **Table 3** and shown in **Fig. 5**. The gneissic granodiorite (XG1-1) has SiO_2 , $\text{MgO} + \text{FeO}^\text{T}$, Na_2O and K_2O contents of 66.54, 2.54, 3.82 and 2.79 wt.%; it has ΣREE contents of 95.9 ppm and shows a large (La/

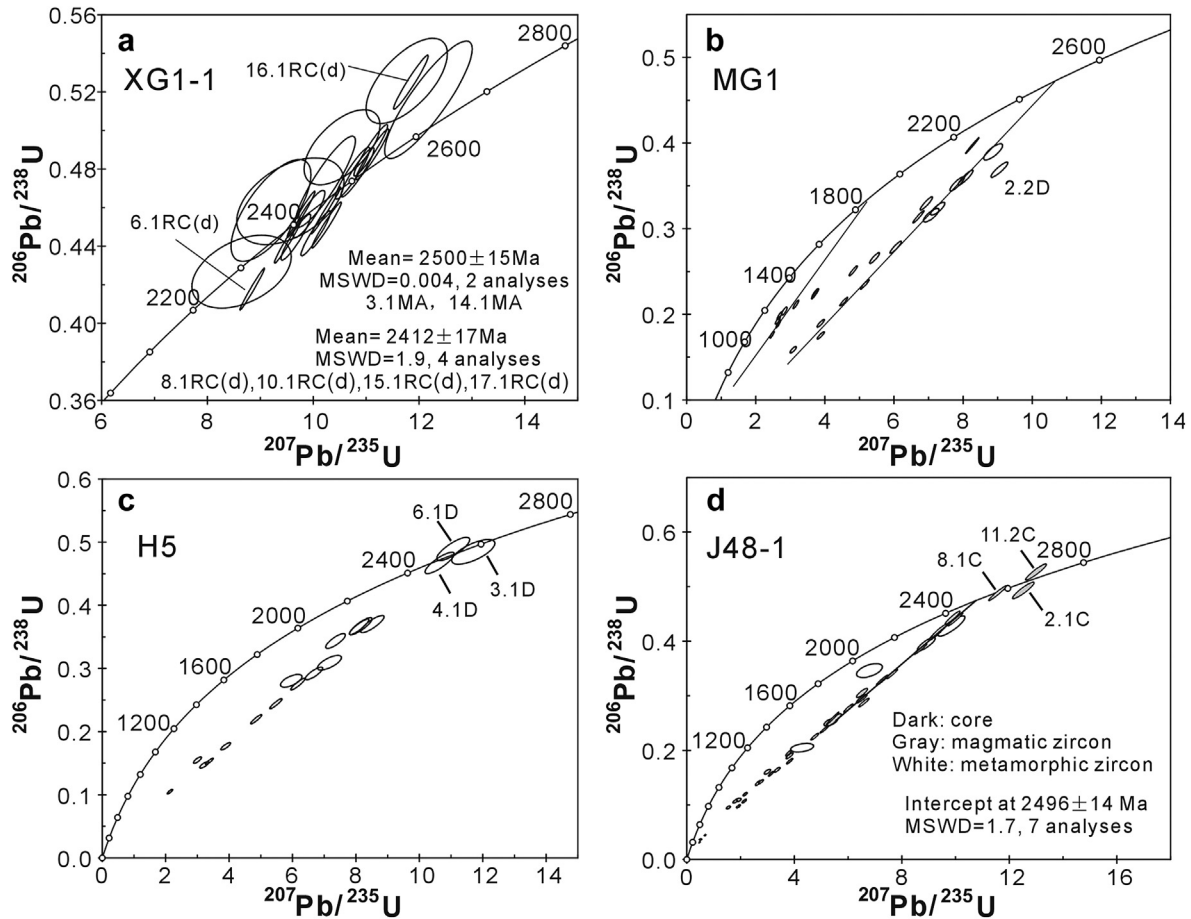


Figure 4. Concordia diagrams showing U-Pb data for zircons from early Precambrian rocks obtained from drill cores beneath the Central Hebei Basin, North China Craton. (a) Gneissic granodiorite (XG1-1); (b) anatectic biotite K-feldspar paragneiss (MG1); (c) muscovite-bearing K-feldspar quartzite (H5); (d) gneissic quartz diorite (J48-1). D, C and RC(d) represent detrital and core zircons and recrystallized dark domains, respectively.

Yb_n ratio (46.1) and positive Eu anomaly (2.35). Compared with the gneissic granodiorite, the gneissic quartz diorite (J48-1) is lower in SiO_2 (61.56 wt.%) and much higher in $\text{MgO} + \text{FeO}^T$ (8.23 wt.%), and has higher ΣREE (140.4 ppm) and lower Eu/Eu^* (0.84) and $(\text{La}/\text{Yb})_n$ (11.5) values. The two metasedimentary samples show large variations in SiO_2 such as 63.06 wt.% (MG1) and 79.77% (H5), respectively, but both are similar in having very high K_2O (6.22–8.72 wt.%) and very low Na_2O contents (0.14–0.30 wt.%). The anatectic biotite K-feldspar paragneiss (MG1) has high $\text{MgO} + \text{FeO}^T$ contents (7.50 wt.%), consistent with its high biotite content. Both samples have ΣREE contents of 48.1–107.6 ppm, Eu/Eu^* of 0.84–0.89 and $(\text{La}/\text{Yb})_n$ of 12.0–29.5. All dated samples are enriched in large ion lithophile (LIL) elements (K, Rb, Ba, Th) (except for sample XG1-1 that has a low Th content) and is depleted in Nb, P and Ti.

5.2. Hf-in-zircon isotopes

In-situ Hf-in-zircon isotopic analyses were obtained from all the dated samples. Analyses were taken on the SHRIMP spots, and we used the $^{207}\text{Pb}/^{206}\text{Pb}$ ages obtained for the dated domains to calculate $\varepsilon_{\text{Hf}}(t)$ values. The results are listed in Table 4 and shown in Fig. 6.

Three analyses on magmatic zircons from gneissic granodiorite sample XG1-1 have $\varepsilon_{\text{Hf}}(t)$ values of 1.21–2.89 and crustal Hf model ages $t_{\text{DM2(CC)}}$ of 2.8–2.9 Ga. Eleven analyses on magmatic zircons from gneissic quartz diorite sample J48-1 have $\varepsilon_{\text{Hf}}(t)$ values and

$t_{\text{DM2(CC)}}$ ages ranging from –1.57 to 4.47 and 2.6 to 2.9 Ga, respectively. The xenocrystic zircons have $t_{\text{DM2(CC)}}$ ages of 2.9–3.0 Ga (spots 2-1C, 8-1C). For the two magmatic rocks, the recrystallized zircon domains show similar Hf isotopic compositions to the magmatic zircons. This suggests that the Lu-Hf isotopic system was not disturbed during metamorphism. Detrital zircons from the two metasedimentary samples have $\varepsilon_{\text{Hf}}(t)$ values and $t_{\text{DM2(CC)}}$ ages ranging from –3.34 to 5.74 and 2.7 to 3.0 Ga, respectively, but those from sample H5 show stronger depletion in Hf isotopes. The somewhat large $\varepsilon_{\text{Hf}}(t)$ variations in these zircons are mainly due to $^{207}\text{Pb}/^{206}\text{Pb}$ age variations because of lead loss. Given an age of 2.5 Ga to calculate $\varepsilon_{\text{Hf}}(t)$, the values are mainly between 0 and 5, with most zircons having $t_{\text{DM2(CC)}}$ ages of 2.7–2.9 Ga.

6. Discussion

We identified ~2.5 Ga old granodiorite and quartz diorite although their spatial distribution is uncertain. The granodiorite (XG1-1) has a relatively high K_2O content (2.79 wt.%) and low $\text{MgO} + \text{FeO}^T$ (2.54 wt.%) and Cr (19 ppm) contents and shows a positive Eu^*/Eu anomaly (2.35). Combined with the magmatic zircons having low $\varepsilon_{\text{Hf}}(t)$ values (1.2–2.9), the rock is considered to be derived from, or at least partly influenced by, continental material. Its strongly fractionated REE pattern does not mean that it formed by partial melting of a basaltic source under high pressure conditions but reflects the compositional feature of a continental source

Table 3

Chemical compositions of early Precambrian rocks from drill cores beneath the Central Hebei Basin, North China Craton.

Sample No.	XG1-1	MG1	H5	J48-1
Rock type	Gneissic granodiorite	Anatetic biotite K-feldspar gneiss	Muscovite-bearing K-feldspar quartz schist	Gneissic quartz diorite
SiO ₂	66.54	63.06	79.77	61.56
TiO ₂	0.21	0.41	0.12	0.48
Al ₂ O ₃	14.59	14.26	9.63	15.23
Fe ₂ O ₃	2.13	1.40	1.05	1.64
FeO	1.74	3.79	0.52	4.58
MnO	0.08	0.04	0.05	0.11
MgO	0.80	2.45	0.70	2.17
CaO	4.84	1.25	0.13	2.48
Na ₂ O	3.82	0.30	0.14	3.40
K ₂ O	2.79	8.72	6.22	2.96
P ₂ O ₅	0.10	0.14	0.05	0.16
H ₂ O ⁺	1.00	2.68	0.84	2.64
CO ₂	0.70	1.25	0.08	2.50
Total	99.3	99.8	99.3	99.9
Cr	19	209	17	100
Ni	7	41	11	35
Sc	4	12	3	15
Rb	37	114	182	105
Ba	1040	2391	729	589
Sr	1413	157	86	271
Zr	76	119	92	137
Nb	1.6	5.3	4.2	6.9
Ta	0.1	0.4	0.4	0.6
Hf	1.8	3.1	2.4	3.8
Y	4.7	4.9	4.1	17.8
Th	0.1	5.6	4.1	8.2
U	<0.05	0.7	1.7	2.5
La	28.00	24.60	9.26	30.80
Ce	42.70	49.40	18.80	59.70
Pr	4.11	5.51	3.02	6.92
Nd	13.90	19.50	11.30	25.20
Sm	1.96	3.00	1.98	4.41
Eu	1.39	0.76	0.45	1.12
Gd	1.59	2.05	1.16	3.67
Tb	0.18	0.23	0.16	0.56
Dy	0.89	1.05	0.73	3.16
Ho	0.18	0.19	0.14	0.63
Er	0.45	0.61	0.45	1.90
Tm	0.06	0.08	0.06	0.26
Yb	0.40	0.55	0.51	1.76
Lu	0.07	0.09	0.08	0.26
ΣREE	95.9	107.6	48.1	140.4
(La/Yb)n	46.1	29.5	12.0	11.5
Eu/Eu*	2.35	0.89	0.84	0.84

Note: major elements in %, trace elements in ppm.

region. The quartz diorite (J48-1) has high MgO + FeO^T (8.23 wt.%) and Cr (100 ppm) contents with a weakly fractionated REE but high ΣREE pattern. It seems to have formed as a result of crystallization-differentiation of more mafic magma, possibly indicating a juvenile

addition of crust from a mantle source. On the other hand, the rock contains 2.6–2.7 Ga xenocrystic zircon cores, and the magmatic zircons have low $\epsilon_{\text{Hf}}(t)$ values, not only suggesting that early Neoarchean rocks occur in the basement but also that these were involved in ~2.5 Ga magmatism. The ~2.5 Ga granodiorite and quartz diorite also occur in other areas of the NCC such as western Shandong and eastern Hebei, where ~2.5 Ga tonalite, trondhjemite, monzogranite and syenogranite are widely distributed (Geng et al., 2006; Yang et al., 2008; Wan et al., 2010, 2011b; Nutman et al., 2011). We speculate that these rock types may also occur in the basement beneath the CHB.

Most detrital zircons from the two metasedimentary samples have ages of ~2.5 Ga. This suggests that the source region is almost entirely composed of late Neoarchean rocks. However, detrital zircons from the muscovite-bearing K-feldspar quartzite (H5) show large variations in internal texture, and this may suggest a certain diversity of rock types and metamorphic grade in the source region. Many detrital zircons show strong lead loss due to high U and Th contents and have ϵ_{Hf} (2.5 Ga) values ranging from 0 to 5. We suggest that the detrital material was derived from a source region that is mainly composed of granitoids derived from crustal reworking of late Mesoarchean to early Neoarchean continental material such as the Archean basement around the basin. In this study, no detrital zircons younger than ~2.5 Ga have been identified, and the metamorphic zircons are ~1.8 Ga in age. Therefore, we are able to constrain the time of deposition for the sedimentary rocks between ~1.8 and 2.5 Ga. More work is required to determine whether the sedimentary rocks were deposited during the early to middle Paleoproterozoic such as the Daqingshan supracrustal rocks in the Daqingshan area (Wan et al., 2009; Dong et al., 2014) and the Shangtaihua Group in the Lushan area (Wan et al., 2006a), or during the late Paleoproterozoic such as the khondalites which are widely distributed in the northern NCC (Wan et al., 2006b; Santosh et al., 2009; Zhao et al., 2010; Dong et al., 2012).

All dated rocks of this study underwent metamorphism and deformation. The gneissic quartz diorite sample (J48-1) recorded a metamorphic age of ~2.5 Ga. The recrystallized dark domains of zircons from the gneissic granodiorite sample (XG1-1) have ²⁰⁷Pb/²⁰⁶Pb ages ranging from 2.4 to 2.5 Ga. The metamorphic age of ~2.4 Ga recorded in sample XG1-1 has also been identified elsewhere in the NCC, but its geological meaning is still uncertain (Dong et al., 2014, references therein). No precise ages for metamorphic zircons have been obtained for the metasedimentary rocks (MG1, H5) that were deposited during the Paleoproterozoic. However, they underwent a tectono-thermal event at the end of the Paleoproterozoic, as discussed above.

We summarized the common features of the NCC basement in the introduction. It is evident that the basement beneath the CHB is similar in many aspects to the basement elsewhere in the NCC.

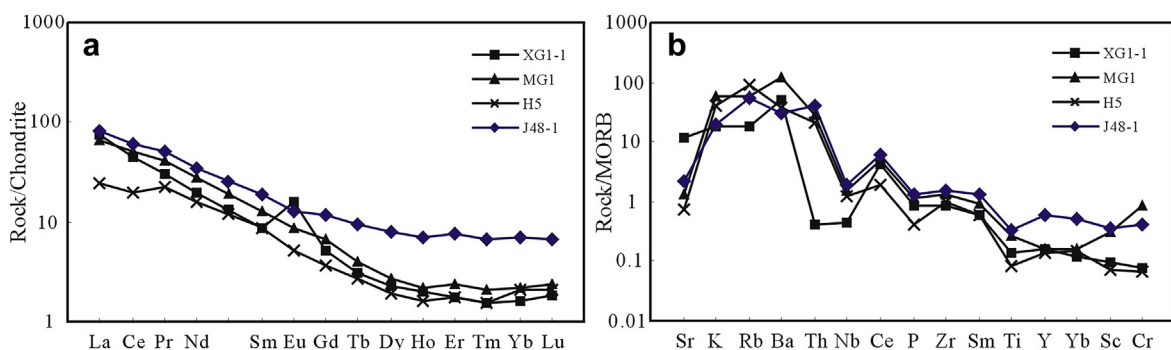


Figure 5. REE patterns (a) and trace element diagrams (b) of early Precambrian rocks obtained from drill cores beneath the Central Hebei Basin, North China Craton.

Table 4

LA-ICPMS Hf isotope data for zircons from early Precambrian rocks from drill cores beneath the Central Hebei Basin, North China Craton.

No.	Age	Discordant (%)	$^{176}\text{Yb}/^{177}\text{Hf}$	$^{176}\text{Lu}/^{177}\text{Hf}$	$^{176}\text{Hf}/^{177}\text{Hf}$	$\pm 2\sigma$	$\epsilon_{\text{Hf}}(0)$	$\epsilon_{\text{Hf}}(t)$	$\pm 2\sigma$	t_{DM1}	$\pm 2\sigma$	$t_{\text{DM2(CC)}}$	$\pm 2\sigma$	$f_{\text{Lu/Hf}}$
Gneissic granodiorite (XG1-1)														
1-1RC(d)	2489	4	0.035412	0.000776	0.281237	0.000015	-54.29	0.25	0.52	2792	40	2890	64	-0.98
3-1MA	2500	-3	0.043179	0.000941	0.281265	0.000019	-53.30	1.21	0.68	2766	52	2850	83	-0.97
4-1RC(I)	2422	-3	0.029061	0.000608	0.281287	0.000017	-52.53	0.79	0.60	2713	45	2808	73	-0.98
6-1RC(d)	2386	6	0.050176	0.001087	0.281321	0.000023	-51.30	0.44	0.80	2699	62	2797	98	-0.97
7-1RC(I)	2570	-4	0.012013	0.000235	0.281249	0.000018	-53.85	3.47	0.63	2737	47	2794	77	-0.99
8-1RC(d)	2404	-1	0.039241	0.000847	0.281276	0.000023	-52.91	-0.38	0.83	2744	64	2853	102	-0.97
8-2RC(I)	2298	-5	0.016614	0.000320	0.281249	0.000018	-53.86	-2.90	0.62	2743	47	2893	76	-0.99
9-1MA	2488	-1	0.041452	0.000842	0.281315	0.000022	-51.54	2.89	0.77	2691	58	2756	93	-0.97
10-1RC(d)	2432	3	0.061930	0.001216	0.281315	0.000022	-51.51	1.04	0.78	2717	60	2804	95	-0.96
11-1RC(I)	2484	-9	0.016299	0.000317	0.281305	0.000021	-51.87	3.35	0.73	2668	55	2730	89	-0.99
12-1RC(d)	2189	36	0.051758	0.001217	0.281365	0.000023	-49.76	-2.61	0.81	2649	63	2790	99	-0.96
14-1MA	2501	-1	0.042799	0.000887	0.281274	0.000021	-52.97	1.66	0.74	2749	56	2828	90	-0.97
15-1RC(d)	2413	2	0.062073	0.001248	0.281303	0.000022	-51.94	0.13	0.79	2736	61	2834	97	-0.96
Anatectic biotite K-feldspar gneiss (MG1)														
2-2D	2634	23	0.087679	0.001479	0.281193	0.000024	-55.84	0.71	0.85	2904	66	2984	103	-0.96
4-2D	2402	27	0.112868	0.002080	0.281312	0.000027	-51.63	-1.16	0.97	2784	77	2890	119	-0.94
5-1D	2485	20	0.048654	0.000892	0.281352	0.000024	-50.23	4.05	0.84	2645	64	2695	103	-0.97
6-1D	2508	16	0.057438	0.001074	0.281235	0.000025	-54.34	0.12	0.91	2816	69	2911	110	-0.97
9-1D	2461	58	0.170546	0.002988	0.281365	0.000031	-49.74	0.49	1.12	2777	90	2855	136	-0.91
11-1D	2386	47	0.145312	0.002741	0.281352	0.000029	-50.22	-1.16	1.04	2778	84	2877	127	-0.92
14-1D	2446	44	0.152903	0.003835	0.281306	0.000029	-51.85	-3.34	1.05	2931	86	3035	127	-0.88
16-1D	2482	29	0.071434	0.002006	0.281291	0.000022	-52.38	-0.05	0.78	2808	62	2899	95	-0.94
18-1D	2329	52	0.125614	0.002430	0.281366	0.000023	-49.73	-1.38	0.83	2735	66	2842	101	-0.93
19-1RC	1636	27	0.073282	0.002219	0.281364	0.000030	-49.80	-15.87	1.08	2722	85	3016	131	-0.93
Muscovite-bearing K-feldspar quartzite (H5)														
1-1D	2483	43	0.033560	0.000721	0.281306	0.000018	-51.86	2.66	0.63	2695	48	2764	76	-0.98
2-1D	2319	72	0.071698	0.001333	0.281386	0.000024	-49.03	0.84	0.85	2628	66	2722	104	-0.96
3-1D	2607	2	0.035969	0.000694	0.281312	0.000025	-51.63	5.74	0.91	2685	69	2710	110	-0.98
4-1D	2509	2	0.027983	0.000550	0.281284	0.000022	-52.63	2.76	0.77	2713	58	2780	94	-0.98
5-1D	2526	20	0.013242	0.000268	0.281319	0.000023	-51.39	4.87	0.81	2646	61	2687	99	-0.99
6-1D	2498	-3	0.015315	0.000322	0.281280	0.000022	-52.75	2.77	0.79	2701	59	2770	96	-0.99
7-1D	2460	48	0.040991	0.000769	0.281334	0.000020	-50.86	3.05	0.70	2660	53	2725	86	-0.98
8-1D	2452	57	0.109854	0.001921	0.281359	0.000029	-49.99	1.84	1.03	2708	81	2780	126	-0.94
9-1D	2438	64	0.061044	0.001120	0.281344	0.000027	-50.49	2.36	0.96	2670	74	2742	117	-0.97
10-1D	2516	34	0.037189	0.000695	0.281325	0.000023	-51.18	4.13	0.83	2667	63	2716	101	-0.98
12-1D	2459	63	0.093736	0.001735	0.281404	0.000026	-48.39	3.91	0.93	2632	73	2681	114	-0.95
13-1D	2539	32	0.030138	0.000587	0.281316	0.000022	-51.51	4.51	0.77	2672	58	2716	94	-0.98
Gneissic quartz diorite (J48-1)														
1-1MA	2368	37	0.024617	0.000567	0.281253	0.000011	-53.73	-1.57	0.39	2756	29	2883	47	-0.98
2-1C	2690	4	0.074362	0.001388	0.281244	0.000021	-54.03	3.94	0.73	2827	56	2868	89	-0.96
4-2MA	2487	11	0.029414	0.000686	0.281290	0.000016	-52.39	2.27	0.56	2713	43	2786	68	-0.98
5-1RC(d)	1973	67	0.057452	0.001372	0.281331	0.000017	-50.94	-8.75	0.62	2706	48	2926	75	-0.96
7-2RC(d)	2220	61	0.054240	0.001252	0.281341	0.000017	-50.60	-2.80	0.60	2684	46	2825	73	-0.96
8-1C	2576	1	0.034594	0.000669	0.281160	0.000019	-57.01	-0.33	0.69	2888	52	2989	84	-0.98
9-1MA	2489	15	0.108535	0.001966	0.281302	0.000026	-51.97	0.57	0.91	2789	72	2873	111	-0.94
11-1RC(d) + R	1646	86	0.088098	0.001690	0.281342	0.000021	-50.55	-15.84	0.74	2713	58	3022	90	-0.95
12-2MA	2516	35	0.036388	0.000805	0.281287	0.000016	-52.51	2.60	0.59	2726	45	2793	71	-0.98
14-1MA	2503	6	0.066984	0.001304	0.281348	0.000021	-50.34	3.64	0.75	2678	58	2730	91	-0.96
15-1MA	2482	9	0.030570	0.000740	0.281283	0.000016	-52.66	1.79	0.58	2727	44	2806	71	-0.98
17-1MA	2405	43	0.069090	0.001329	0.281344	0.000027	-50.50	1.27	0.95	2685	74	2770	116	-0.96
18-1RC(d)	2484	24	0.041602	0.000905	0.281226	0.000022	-54.66	-0.45	0.78	2815	59	2920	95	-0.97
20-1MA	2460	26	0.041136	0.000906	0.281310	0.000023	-51.69	1.99	0.83	2702	63	2778	101	-0.97
26-1MA	2474	4	0.030802	0.000717	0.281265	0.000019	-53.29	1.02	0.67	2750	51	2839	81	-0.98
29-1MA	2451	32	0.062967	0.001218	0.281400	0.000017	-48.51	4.47	0.62	2601	48	2646	75	-0.96
30-1RC(d)	2422	35	0.050939	0.001223	0.281324	0.000019	-51.21	1.11	0.66	2705	51	2792	80	-0.96
32-1MA	2381	45	0.054541	0.001075	0.281338	0.000023	-50.70	0.95	0.80	2675	62	2767	98	-0.97
1-1MA	2368	37	0.024617	0.000567	0.281253	0.000011	-53.73	-1.57	0.39	2756	29	2883	47	-0.98
2-1C	2690	4	0.074362	0.001388	0.281244	0.000021	-54.03	3.94	0.73	2827	56	2868	89	-0.96
4-2MA	2487	11	0.029414	0.000686	0.281290	0.000016	-52.39	2.27	0.56	2713	43	2786	68	-0.98
5-1RC(d)	1973	67	0.057452	0.001372	0.281331	0.000017	-50.94	-8.75	0.62	2706	48	2926	75	-0.96
7-2RC(d)	2220	61	0.054240	0.001252	0.281341	0.000017	-50.60	-2.80	0.60	2684	46	2825	73	-0.96
8-1C	2576	1	0.034594	0.000669	0.281160	0.000019	-57.01	-0.33	0.69	2888	52	2989	84	-0.98
9-1MA	2489	15	0.108535	0.001966	0.281302	0.000026	-51.97	0.57	0.91	2789	72	2873	111	-0.94
11-1RC(d) + R	1646	86	0.088098	0.001690	0.281342	0.000021	-50.55	-15.84	0.74	2713	58	3022	90	-0.95
12-2MA	2516	35	0.036388	0.000805	0.281287	0.000016	-52.51	2.60	0.59	2726	45	2793	71	-0.98

(continued on next page)

Table 4 (continued)

No.	Age	Discordant (%)	$^{176}\text{Yb}/^{177}\text{Hf}$	$^{176}\text{Lu}/^{177}\text{Hf}$	$^{176}\text{Hf}/^{177}\text{Hf}$	$\pm 2\sigma$	$\epsilon_{\text{Hf}}(0)$	$\epsilon_{\text{Hf}}(t)$	$\pm 2\sigma$	t_{DM1}	$\pm 2\sigma$	$t_{\text{DM2(CC)}}$	$\pm 2\sigma$	$f_{\text{Lu/Hf}}$
14-1MA	2503	6	0.066984	0.001304	0.281348	0.000021	-50.34	3.64	0.75	2678	58	2730	91	-0.96
15-1MA	2482	9	0.030570	0.000740	0.281283	0.000016	-52.66	1.79	0.58	2727	44	2806	71	-0.98
17-1MA	2405	43	0.069090	0.001329	0.281344	0.000027	-50.50	1.27	0.95	2685	74	2770	116	-0.96
18-1RC(d)	2484	24	0.041602	0.000905	0.281226	0.000022	-54.66	-0.45	0.78	2815	59	2920	95	-0.97
20-1MA	2460	26	0.041136	0.000906	0.281310	0.000023	-51.69	1.99	0.83	2702	63	2778	101	-0.97
26-1MA	2474	4	0.030802	0.000717	0.281265	0.000019	-53.29	1.02	0.67	2750	51	2839	81	-0.98
29-1MA	2451	32	0.062967	0.001218	0.281400	0.000017	-48.51	4.47	0.62	2601	48	2646	75	-0.96
30-1RC(d)	2422	35	0.050939	0.001223	0.281324	0.000019	-51.21	1.11	0.66	2705	51	2792	80	-0.96
32-1MA	2381	45	0.054541	0.001075	0.281338	0.000023	-50.70	0.95	0.80	2675	62	2767	98	-0.97

Note: (1) In-situ Hf isotopic analyses were carried out on the same spots as zircon dating; (2) age in Ma; (3) MA, D, C, RC(d) and RC(l) represent magmatic, detrital and core zircons and recrystallized dark and light domains, respectively.

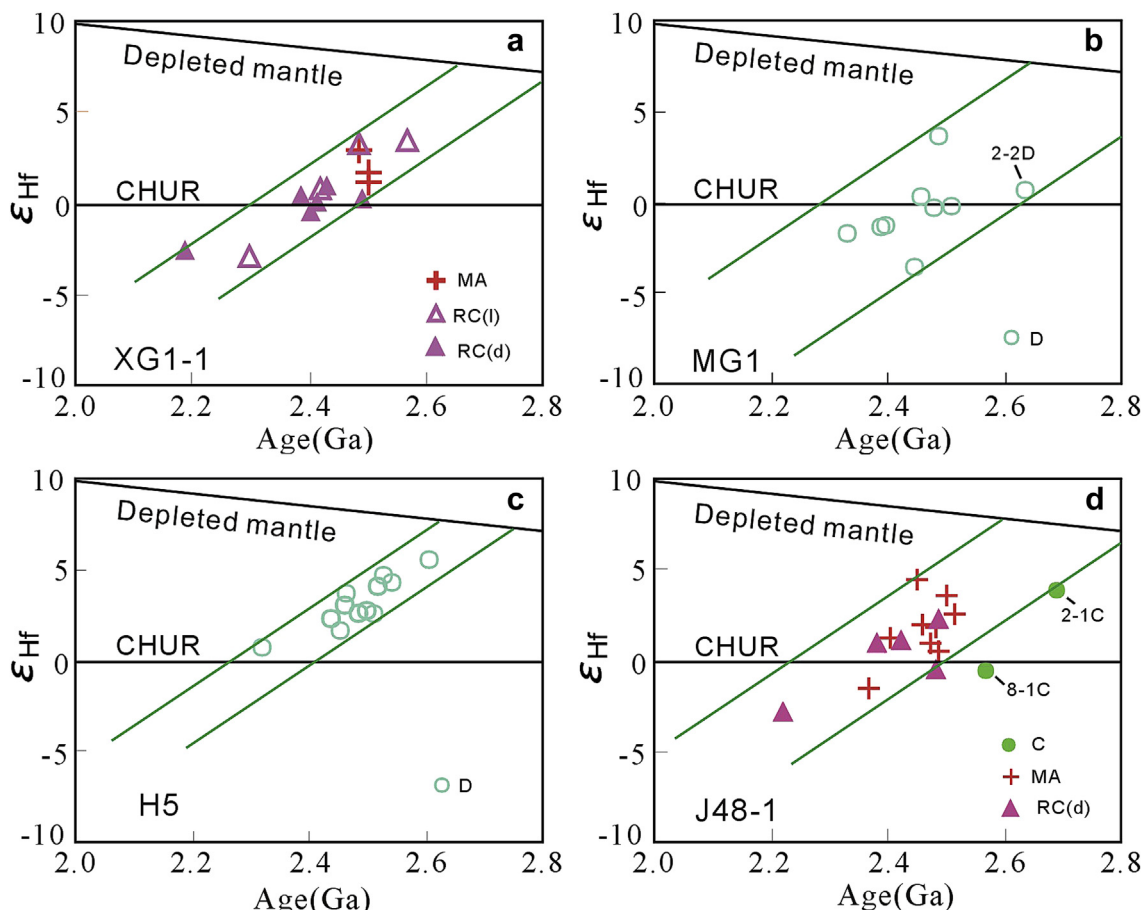


Figure 6. Age versus $\epsilon_{\text{Hf}}(t)$ diagrams for zircons from early Precambrian rocks obtained from drill cores beneath the Central Hebei Basin, North China Craton. (a) Gneissic granodiorite (XG1-1); (b) anatetic biotite K-feldspar paragneiss (MG1); (c) muscovite-bearing K-feldspar quartzite (H5); (d) gneissic quartz diorite (J48-1). MA, D, C, RC(d) and RC(l) represent magmatic, detrital and core zircons and recrystallized dark and light domains, respectively.

7. Conclusions

- 1) The basement beneath the CHB contains ~2.5 Ga magmatic and Paleoproterozoic metasedimentary rocks.
- 2) Zircons of different origins yielded ϵ_{Hf} (2.5 Ga) values and Hf crustal modal ages ranging from 0 to 5 and 2.7 to 2.9 Ga, respectively.
- 3) The analyzed samples recorded two tectono-thermal events during the late Neoarchean to early Paleoproterozoic and at the end of the Paleoproterozoic, respectively.
- 4) The early Precambrian basement beneath the CHB is similar in many aspects to that elsewhere in the NCC.

Acknowledgments

This paper expresses our appreciation to the distinguished geologists Guowei Zhang and Alfred Kröner who have made significant contributions to the geology of China. We thank Jianhui Liu for help with SHRIMP data collection, Chun Yang and Weilin Gan for making the zircon mounts, and Liqing Zhou and Ning Li for CL imaging. We thank two anonymous reviewers for their valuable comments. This project was financially supported by the Major State Basic Research Program of the People's Republic of China (Grant No. 2012CB416600), the National Natural Science Foundation of China (Grant No. 40672127) and the Key Program of the

Ministry of Land and Resources of China (Grant Nos. 1212010811033, 12120113013700).

References

- Black, L.P., Kamo, S.L., Allen, C.M., Aleinikoff, J.K., Davis, D.W., Korsch, R.J., Foudoulis, C., 2003. TEMORA 1: a new zircon standard for phanerozoic U–Pb geochronology. *Chemical Geology* 200, 155–170.
- Blichert-Toft, J., Albarède, F., 1997. The Lu–Hf isotope geochemistry of chondrites and the evolution of the mantle–crust system. *Earth and Planetary Science Letters* 148, 243–258.
- Cheng, Y.Q., Yang, C.H., Wan, Y.S., Liu, Z.X., Zhang, X.P., Du, L.L., Zhang, S.G., Wu, J.S., Gao, J.F., 2004. Early Precambrian Geological Characters and Anatetic Reconstruction of Crust in North Part of Middle Taihang Mountain. Geological Publishing House, Beijing, 191pp (in Chinese).
- Dong, C.Y., Wan, Y.S., Xu, Z.Y., Liu, D.Y., Yang, Z.S., Ma, M.Z., Xie, H.Q., 2012. Late Paleoproterozoic kondalites in the Daqingshan area, North China Craton: SHRIMP zircon U–Pb dating. *Science China Earth Sciences* 55, 1–11.
- Dong, C.Y., Wan, Y.S., Wilde, S.A., Xu, Z.Y., Ma, M.Z., Xie, H.Q., Liu, D.Y., 2014. Early Paleoproterozoic supracrustal rocks at Daqingshan in the khondalite belt of North China Craton: evidence from SHRIMP zircon U–Pb dating. *Gondwana Research*. <http://dx.doi.org/10.1016/j.gr.2013.05.021>.
- Geng, Y.S., Liu, F.L., Yang, C.H., 2006. Magmatic event at the end of the Archean in Eastern Hebei province and its geological implication. *Acta Geologica Sinica* 80, 819–833.
- Griffin, W.L., Pearson, N.J., Belousova, E., Jackson, S.E., Achterbergh, E.V., O'Reilly, S.Y., Shee, S.R., 2000. The Hf isotope composition of cratonic mantle: LAM-MC-ICPMS analysis of zircon megacrysts in kimberlites. *Geochimica et Cosmochimica Acta* 64, 133–147.
- Guan, H., Sun, M., Wilde, S.A., Zhou, X., Zhai, M.G., 2002. SHRIMP U–Pb zircon geochronology of the Fuping complex: implications for formation and assembly of the north China craton. *Precambrian Research* 113, 1–18.
- Han, B.F., Xu, Z., Ren, R., Li, L.L., Yang, J.H., Yang, Y.H., 2012. Crustal growth and intracrustal recycling in the middle segment of the Trans-North China Orogen, North China Craton: a case study of the Fuping Complex. *Geological Magazine* 149, 729–742.
- Hou, K.J., Li, Y.H., Zou, T.R., Qu, X.M., Shi, Y.R., Xie, G.Q., 2007. Laser ablation-MC-ICP-MS technique for Hf isotope microanalysis of zircon and its geological applications. *Acta Petrologica Sinica* 23, 2595–2604 (In Chinese with English abstract).
- Hu, J.M., Liu, X.S., Li, Z.H., Zhao, Y., Zhang, S.H., Liu, X.C., Qu, H.J., Chen, H., 2012. SHRIMP U–Pb zircon dating of the Ordos Basin basement and its tectonic significance. *Chinese Science Bulletin* 58, 118–127.
- Kröner, A., Rojas-Agramonte, Y., Kehlpannala, K.V.W., Zach, T., Hegner, E., Geng, H.Y., Wong, J., Barth, M., 2013. Age, Nd–Hf isotopes, and geochemistry of the Vijayan Complex of eastern and southern Sri Lanka: a Grenville-age magmatic arc of unknown derivation. *Precambrian Research* 234, 288–321.
- Kröner, A., Kovach, V., Belousova, E., Hegner, E., Armstrong, R., Dolgopolova, A., Seltmann, R., Alexeev, D.V., Hoffmann, J.E., Wong, J., Sun, M., Cai, K., Wang, T., Tong, Y., Wilde, S.A., Degtyarev, K.E., Rytsk, E., 2014. Reassessment of continental growth during the accretionary history of the Central Asian Orogenic Belt. *Gondwana Research* 25, 103–125.
- Ludwig, K.R., 2001. Squid 1.02: A User's Manual: Berkeley Geochronology Centre, Special Publication, 2, p. 19 p.
- Liu, S.J., Wan, Y.S., Sun, H.Y., Nutman, A., Xie, H.Q., Dong, C.Y., Ma, M.Z., Liu, D.Y., Jahn, B.M., 2013. Paleo- to Eoarchean crustal evolution in eastern Hebei, North China Craton: new evidence from SHRIMP U–Pb dating and in-situ Hf isotopic study of detrital zircons from paragneisses. *Journal of Asian Earth Science* 78, 4–17.
- Liu, D.Y., Nutman, A.P., Compston, W., Wu, J.S., Shen, Q.H., 1992. Remnants of 3800 Ma crust in the Chinese part of the Sino-Korean Craton. *Geology* 20, 339–342.
- Ludwig, K.R., 2003. User's Manual for Isoplot 3.00, a Geochronological Toolkit for Microsoft Excel. Berkeley Geochronology Center, 70 p.
- Nasdala, L., Hofmeister, W., Norberg, N., Mattinson, J.M., Corfu, F., Dor, W., Kamo, S.L., Kennedy, A.K., Kronz, A., Reiners, P.W., Frei, D., Kosler, J., Wan, Y.S., Goze, J., Hoer, T., Kröner, A., Valley, J.W., 2008. Zircon M257: a homogeneous natural reference material for the ion microprobe U–Pb analysis of zircon. *Geostandards and Geoanalytical Research* 32, 247–265.
- North China Oilfield Company of PetroChina (NCOCP), 2012. Introduction on Drilling Cores Relating to Precambrian Basement in the Central Hebei Basin. Unpublished ms, 18 p.
- Nutman, A.P., Wan, Y.S., Du, L.L., Friend, C.R.L., Dong, C.Y., Xie, H.Q., Wang, W., Sun, H.Y., Liu, D.Y., 2011. Multistage late Neoarchean crustal evolution of the North China Craton, eastern Hebei. *Precambrian Research* 189, 43–65.
- Pei, F.P., Xu, W.L., Yang, D.B., Zhao, Q.G., Liu, X.M., Hu, Z.C., 2007. Zircon U–Pb geochronology of basement metamorphic rocks in the Songliao Basin. *Chinese Science Bulletin* 52, 942–948.
- Santosh, M., Wan, Y.S., Liu, D.Y., Dong, C.Y., Li, J.H., 2009. Anatomy of zircons from an ultra-hot orogen: suturing the North China Craton within Columbia supercontinent. *Journal of Geology* 117, 429–443.
- Söderlund, U., Patchett, P.J., Vervoort, J.D., Isachsen, C.E., 2004. The ^{176}Lu decay constant determined by Lu–Hf and U–Pb isotope systematics of Precambrian mafic intrusions. *Earth and Planetary Science Letters* 219, 311–324.
- Sun, H.Y., Dong, C.Y., Xie, H.Q., Wang, W., Ma, M.Z., Liu, D.Y., Nutman, A., Wan, Y.S., 2010. The formation age of the Neoarchean Zhuzhangzi and Dantazi Groups in the Qinglong area, eastern Hebei province: evidence from SHRIMP U–Pb zircon dating. *Geological Review* 56, 888–898 (in Chinese with English abstract).
- Trap, P., Faure, M., Lin, W., Monié, P., Bruguier, O., 2008. Contrasted tectonic styles for the Paleoproterozoic evolution of the North China Craton. Evidence for a ~2.1 Ga thermal and tectonic event in the Fuping Massif. *Journal of Structural Geology* 30, 1109–1125.
- Trap, P., Faure, M., Lin, W., Monié, P., Meffre, S., Melletton, J., 2009. The Zanhuan Massif, the second and eastern suture zone of the Paleoproterozoic trans-north China Orogen. *Precambrian Research* 172, 80–98.
- Wan, Y.S., Wilde, S.A., Liu, D.Y., Yang, C.X., Song, B., Yin, X.Y., 2006a. Further evidence for ~1.85 Ga metamorphism in the Central Zone of the North China Craton: SHRIMP U–Pb dating of zircon from metamorphic rocks in the Lushan area, Henan Province. *Gondwana Research* 9, 189–197.
- Wan, Y.S., Song, B., Liu, D.Y., Wilde, S.A., Wu, J.S., Shi, Y.R., Yin, X.Y., Zhou, H.Y., 2006b. SHRIMP U–Pb zircon geochronology of Paleoproterozoic metasedimentary rocks in the North China Craton: evidence for a major Late Paleoproterozoic tectonothermal event. *Precambrian Research* 149, 249–271.
- Wan, Y.S., Liu, D.Y., Dong, C.Y., Xu, Z.Y., Wang, Z.J., Wilde, S.A., Yang, Y.H., Liu, Z.H., Zhou, H.Y., 2009. The Precambrian Khondalite Belt in the Daqingshan area, North China Craton: evidence for multiple metamorphic events in the Palaeoproterozoic. In: Reddy, S.M., Mazumder, R., Evans, D.A.D., Collins, A.S. (Eds.), *Palaeoproterozoic Supercontinents and Global Evolution: Journal of the London Geological Society, Special Publications* 323, pp. 73–97.
- Wan, Y.S., Liu, D.Y., Wang, S.J., Dong, C.Y., Yang, E.X., Wang, W., Zhou, H.Y., Du, L.L., Yin, X.Y., Xie, H.Q., Ma, M.Z., 2010. Juvenile magmatism and crustal recycling at the end of Neoarchean in western Shandong province, north China Craton: evidence from SHRIMP zircon dating. *American Journal of Science* 310, 1503–1552.
- Wan, Y.S., Liu, D.Y., Wang, W., Song, T.R., Kröner, A., Dong, C.Y., Zhou, H.Y., Yin, X.Y., 2011a. Provenance of Meso- to Neoproterozoic cover sediments at the Ming Tombs, Beijing, North China Craton: An integrated study of U–Pb dating and Hf isotopic measurement of detrital zircons and whole-rock geochemistry. *Gondwana Research* 20, 219–242.
- Wan, Y.S., Liu, D.Y., Wang, S.J., Yang, E.X., Wang, W., Dong, C.Y., Zhou, H.Y., Du, L.L., Yang, Y.H., Diwu, C.R., 2011b. 2.7 Ga juvenile crust formation in the North China Craton (Taishan-Xintai area, western Shandong Province): further evidence of an understated event from zircon U–Pb dating and Hf isotope composition. *Precambrian Research* 186, 169–180.
- Wan, Y.S., Xie, H.Q., Yang, H., Wang, Z.J., Liu, D.Y., Kröner, A., Wilde, S.A., Geng, Y.S., Sun, L.Y., Ma, M.Z., Liu, S.J., Dong, C.Y., Du, L.L., 2013. Is the Ordos Block Archean or Paleoproterozoic in age? Implications for the Precambrian evolution of the North China Craton. *American Journal of Science* 313, 683–711.
- Wilde, S.A., Valley, J.W., Kita, N.T., Cavosie, A.J., Liu, D.Y., 2008. SHRIMP U–Pb and CAMECA 1280 Oxygen isotope results from ancient detrital zircons in the Caozhuang Quartzite, Eastern Hebei, North China Craton: evidence for crustal reworking 3.8 Ga ago. *American Journal of Science* 308, 185–199.
- Williams, I.S., 1998. U–Th–Pb geochronology by ion microprobe. In: McKibben, M.A., Shanks, W.C., Ridley, W.I. (Eds.), *Applications of Microanalytical Techniques to Understanding Mineralizing Processes*, 7. *Review in Economic Geology*, pp. 1–35.
- Xiao, L.L., Jiang, Z.S., Wang, G.D., Wan, Y.S., Wang, T., Wu, C.M., 2011. Metamorphic reaction textures and metamorphic P-T-t loops of the Precambrian Zanhuan metamorphic complex, Hebei, North China. *Acta Petrologica Sinica* 27, 980–1002.
- Yang, C.H., Du, L.L., Wan, Y.S., Liu, Z.X., 2004. SHRIMP zircon U–Pb chronology of tonalitic gneiss in Banqiaogou area, Pingshan, Hebei Province. *Geological Journal of China University* 12, 514–522.
- Yang, J.H., Wu, F.Y., Wilde, S.A., Zhao, G.C., 2008. Petrogenesis and geodynamics of Late Archean magmatism in eastern Hebei, eastern North China Craton: geochronological, geochemical and Nd–Hf isotopic evidence. *Precambrian Research* 167, 125–149.
- Yang, C.H., Du, L.L., Ren, L.D., Song, H.X., Wan, Y.S., Xie, H.Q., Liu, Z.X., 2011a. Petrogenesis and geodynamic setting of the Jiāndēng potassiac granite at the end of the neoarchean in the Zanhuan complex, North China Craton. *Earth Science Frontiers* 18, 62–78 (in Chinese with English abstract).
- Yang, C.H., Du, L.L., Ren, L.D., Song, H.X., Wan, Y.S., Xie, H.Q., Liu, Z.X., 2011b. The age and petrogenesis of the Xuting granite in the Zanhuan complex, Hebei province-constraints on the structural evolution of the trans-north China orogen, north China craton. *Acta Petrologica Sinica* 27, 1003–1016 (in Chinese with English abstract).
- Yang, C.H., Du, L.L., Ren, L.D., Song, H.X., Wan, Y.S., Xie, H.Q., Geng, Y.S., 2013. Delineation of the ca. 2.7 Ga TTG gneisses in the Zanhuan Complex, North China Craton and its geological implications. *Journal of Asian Earth Sciences* 72, 178–189.
- Zhai, M.G., Santosh, M., 2011. The early Precambrian odyssey of the North China Craton: a synoptic overview. *Gondwana Research* 20, 6–25.
- Zhang, X.J., Zhang, L.C., Xiang, P., Wan, B., Pirajno, F., 2011. Zircon U–Pb age, Hf isotopes and geochemistry of Shuichang Algoma-type banded iron-formation,

- North China Craton: constraints on the ore-forming age and tectonic setting. *Gondwana Research* 20, 137–148.
- Zhang, L.C., Zhai, M.G., Wan, Y.S., Guo, J.H., Dai, Y.P., Wang, C.L., Liu, L., 2012a. Study of the Precambrian BIF-iron deposits in the North China Craton: progresses and questions. *Acta Petrologica Sinica* 28, 3431–3445 (in Chinese with English abstract).
- Zhang, L.C., Zhai, M.G., Zhang, X.J., Xiang, P., Dai, Y.P., Wang, C.L., Pirajno, F., 2012b. Formation age and tectonic setting of the Shirengou Neoarchean banded iron deposit in eastern Hebei Province: constraints from geochemistry and SIMS zircon U-Pb dating. *Precambrian Research* 222, 325–338.
- Zhao, G.C., Cawood, P.A., Wilde, S.A., Sun, M., Lu, L.Z., 2000. Metamorphism of basement rocks in the central zone of the north China craton: implications for Paleoproterozoic tectonic evolution. *Precambrian Research* 103, 55–88.
- Zhao, G.C., Wilde, S.A., Cawood, P.A., Sun, M., 2002. SHRIMP U–Pb zircon ages of the Fuping complex: implications for Late Archean to Paleoproterozoic accretion and assembly of the North China Craton. *American Journal of Science* 302, 191–226.
- Zhao, G.C., Wilde, S.A., Guo, J.H., Cawood, P.A., Sun, M., Li, X.P., 2010. Single zircon grains record two Paleoproterozoic collisional events in the North China Craton. *Precambrian Research* 177, 266–276.
- Zhao, G.C., Zhai, M.G., 2013. Lithotectonic elements of Precambrian basement in the North China Craton: review and tectonic implications. *Gondwana Research* 23, 1207–1240.